Journal of Inorganic and Organometallic Polymers and Materials (2024) 34:2153–2162
https://doi.org/10.1007/s10904-023-02955-8

RESEARCH

ZnO Nanoparticle-Enhanced Electrochemical Sensor Utilizing Moringa *Oleifera* Leaf Extract for Real-Time Dopamine Detection

M. Manikandan[1,2] · G. Lakshmi Priya[1,2] · E. Manikandan[1,2] · Vithyasaahar Sethumadhavan[3]

Received: 7 October 2023 / Accepted: 21 November 2023 / Published online: 3 January 2024

Abstract
Using an extract from the leaves of the Moringa *Oleifera* tree as a sustainable reducing and stabilizing agent, this research details a unique method for synthesizing zinc oxide (ZnO) nanoparticles. With the synthesized ZnO nanoparticles, a sensitive electrochemical sensor for detecting dopamine was developed. By exploiting the bioactive components found in Moringa *Oleifera* leaf extract, green production of ZnO nanoparticles was achieved, providing a chemical-free alternative. The nanoparticles' structural and morphological features were deduced with the aid of analytical methods like X-ray diffraction (XRD), Fourier-transform infrared spectroscopy (FTIR), Ultra Violet Visible spectroscopy (UV–Vis), scanning electron microscopy (SEM), transmission electron microscopy (TEM), atomic force spectroscopy (AFM) and X-ray photoelectron spectroscopy (XPS). The electrochemical sensor was built by incorporating the synthesized ZnO nanoparticles onto a Glassy Carbon Electrode. The sensor is sensitive and selective to dopamine, a neurotransmitter involved in many physiological and neurological functions. We employed electrochemical methods like cyclic voltammetry, square wave voltammetry and electrochemical impedance spectroscopy to analyze dopamine molecules' interactions with the ZnO nanoparticle-modified electrode. We found that neurotransmitter binding affects the sensor's electrical response. The vast linear detection range and low dopamine detection limit make the electrochemical sensor helpful for basic neuroscience research and clinical diagnosis. ZnO nanoparticles synthesized ecologically showed promise as efficient sensing materials and the practicality of such approaches. As a whole, this research demonstrates the complementary relationship between green chemistry, nanotechnology, and electrochemical sensing, with potential for use in the creation of environmentally friendly sensors and the enhancement of dopamine detection.

Keywords Green synthesis · Dopamine detection · M. *oleifera* · Zinc oxide · Electrochemical sensor

1 Introduction

Dopamine is a vital neurotransmitter with profound implications for human psychology, behavior, and overall well-being. It is essential to comprehend its function and control its levels while contemplating the mental health, neurological disorders, addiction, and various aspects of human behavior and cognition [1–3]. Electrochemical sensors make it possible to measure dopamine levels in both real-time and in continuous fashion. This phenomenon holds particular significance in scenarios characterized by dynamic fluctuations in dopamine levels, such as instances involving stress-induced reactions, rewarding encounters, or cognitive acquisition. The performance of electrochemical dopamine sensors is significantly impacted by the selection of electrode material. In 2010, Nada F. Atta presented an electrochemical sensor that detects Dopamine (DA) in a universal buffer solution (pH 7.4) with Ascorbic Acid (AA) and Uric Acid (UA). Gold nanoparticle-modified carbon paste electrodes power the sensor. Unlike AA and UA, the sensor responds only to DA [4]. Carbon-based materials, such as graphene, carbon nanotubes, and graphite, possess notable characteristics such as a large surface area, superior electrical conductivity, and convenient functionalization capabilities [5–7]. In the past decade, noble metals like gold and

✉ G. Lakshmi Priya
lakshmipriya.g@vit.ac.in

1 Centre for Innovation and Product Development, Vellore Institute of Technology, Chennai 600127, India

2 School of Electronics Engineering, Vellore Institute of Technology, Chennai 600127, India

3 School of Chemistry and Physics, Queensland University of Technology, (QUT), Brisbane City, Australia

platinum have been recognized for their exceptional electrocatalytic performance in dopamine oxidation. Simultaneously, 2D nanomaterials, including graphene [8], reduced Graphene Oxide (rGO), Carbon Nanotubes (CNTs) [9, 10], magnetic nanomaterials [11] and conducting polymers [12], have surfaced in numerous forms. The 2D nanomaterials stand out due to their superior electrical conductivity in the creation of highly sensitive biosensors. However, nanostructured materials, such as metal oxides ZnO and MnO_2, exhibit an increased sensitivity due to their ability to offer a large number of active sites for the adsorption of dopamine. Dopamine (DA) detection using an electrochemical sensor that does not require enzymes is a unique approach reported by Chedia et al. in 2020. With the help of cyclic voltammetry, graphene oxide and nickel nanoparticles were deposited as a composite on a Glassy Carbon Electrode (GCE) [13]. The modified electrode has a sensitivity of 0.641 AM^{-1} and a detection limit of 10^{-7} M. The results show high selectivity despite the presence of competitive chemicals like uric acid, ascorbic acid, and glucose. Non-enzymatic dopamine sensing applications may benefit from this low-cost and simple-to-fabricate electrodeposited graphene oxide electrode. DNA-based nanoprobes for ultrasensitive and selective dopamine detection have also been recently reported [14]. Signal amplification is achieved in part by the high surface area and unusual electron transport capabilities of quantum dots, nanoparticles, and nanocomposites. Sensor specificity is enhanced when these nanoparticles are functionalized with recognition components. The rapid electron transfer kinetics of ZnO nanoparticles enables electrochemical sensors to provide real-time or near-real-time detection of dopamine [15]. This is particularly important for applications that require monitoring rapid changes in dopamine levels. ZnO exhibits excellent electrochemical properties, making it an ideal material for modifying electrode surfaces in electrochemical sensors [16]. Zinc oxide (ZnO) nanoparticles have gained significant attention in the field of biosensors [17–21] due to their unique properties and potential applications. They are particularly useful in the development of biosensors for various analytes, including dopamine, a neurotransmitter involved in several physiological processes. The conductive nature of ZnO allows efficient electron transfer between the electrode and dopamine molecules, leading to a strong electrochemical response. The synthesis of ZnO nanoparticles has been a subject of extensive research, with a focus on tailoring their size, shape, and properties to meet specific application requirements [22]. Synthesis of ZnO nanoparticles has been attempted in a variety of ways, the earliest of which include chemical precipitation and hydrothermal processes [23]. These procedures are easy to implement and can be expanded upon. Modulating reaction conditions like temperature, pH, and precursor concentrations allows for precise manipulation of particle size and morphology. Sol-gel techniques involve the production of nanoparticles through the transformation of precursor sols into a gel-like network and subsequent thermal treatment. Particle size and composition can be precisely managed with this method [24, 25]. Green synthesis techniques have become increasingly popular in recent years due to the fact that they are less destructive to the environment and have the potential to produce sustainable nanomaterials [26, 27]. In order to produce zinc oxide nanoparticles in an environmentally friendly manner, Moringa *Oleifera* leaf extract, which is abundant in bioactive components, has been utilized. The utilization of Moringa *Oleifera* leaf extract to synthesize ZnO nanoparticles with excellent catalytic activity for dye degradation was reported [28]. The reduction of zinc precursors in the presence of bio-based reducing agents, such as plant extracts, is an important step in the environmentally friendly synthesis of ZnO nanoparticles. The biomolecules that are contained in these extracts, such as polyphenols, flavonoids, and terpenoids, perform the functions of reducing and capping agents, making it easier for ZnO nanoparticles to nucleate and proliferate [29, 30]. Plectranthus amboinicus plant extract was also reported in use to synthesize ZnO nanoparticles to examine its anti-bacterial properties [31]. Wen-Hui Zhou et al. had incorporated AuNPs into the ZnO nanorods arrays to improve the sensitivity, selectivity, and efficiency of dopamine detection through the synergistic effects of these two nanomaterials [32]. In 2021, Li et al. presented a novel electrochemical sensing strategy that integrates ZnO nanorods and electro-reduced graphene oxide (ERGO) into a composite material for enhancing the detection of dopamine [33]. Focusing on the special features that allow for selective and sensitive sensing, the potential of chiral ZnO nanoparticles in the realm of dopamine detection has also been investigated [34]. For the detection of dopamine, researchers have also reported a design for an electrochemical sensor that relied on a three-dimensional composite of reduced graphene oxide (rGO) and zinc oxide (ZnO). The goal of this study is to improve the sensor's sensitivity to dopamine by exploiting the specific characteristics of the rGO/ZnO combination [35, 36]. Similarly, development of a sensor for dopamine detection using ZnO modified carbon paste and ZnO—carbon nanofiber have also been reported to understand its electrochemical behavior [37]. Also, there are numerous analytical and electroanalytical methods [38] that can be adapted for various applications, ranging from detection of biomarkers, environmental analysis to materials characterization and quality control in industries. The use of a screen-printed graphite electrode modified with a Ni-Mo-based Metal-Organic Framework (MOF) for the voltammetric determination of the food dye amaranth was reported by S.Tajit et. al. that has shown appreciable electrochemical oxidation with higher sensitivity of 0.0671 $\mu A\ \mu M^{-1}$ [39]. The author had also reported various

electrochemical sensor works for the detection of mangiferin [40], N-acetylcysteine and Folic Acid [41] using Sqaure Wave Voltammetry (SWV) technique. As our understanding of the importance of dopamine expands, there will be an increasing need for accurate and sensitive detection techniques. This will establish electrochemical sensors as indispensable instruments in both scientific investigations and real-world scenarios. Dopamine detection research utilizing green-synthesized zinc oxide (ZnO) nanoparticles will address the demand for ecologically responsible and long-term solutions in the realm of sensor technology. The production of ZnO nanoparticles can be achieved through green synthesis techniques, utilizing natural sources like plant extracts rather than energy-intensive and potentiallyhazardous chemical processes. This study seeks to enhance the performance of electrochemical sensors for dopamine detection by harnessing the unique attributes of environmentally friendly-synthesized ZnO nanoparticles.

2 Materials and Methods

2.1 Synthesis of ZnO Using Moringa *Oleifera* Leaf Extract

Moringa *Oleifera* leaves were collected and scrubbed with tap water and distilled water to remove unwanted impurities like dust particles and other contamination. The leaf sample was dried at room temperature for synthesis purposes. Zinc nitrate hexahydrate (Zn $(NO_3)_2{\cdot}6H_2O$), di-sodium hydrogen phosphate anhydrous (Na_2HPO_4), monosodium phosphate (NaH_2PO_4), sodium chloride (NaCl) and double distilled water were used as the precursor for the preparation of ZnO and phosphate buffer solution (PBS). Every substance utilized were analytical grade and acquired from Sigma Aldrich. 5 g of leaf was baked with 100 ml of distilled water for 2 h at 60 °C. A light yellow-colored solution was created during the boiling process and was cooled to room temperature. Using Whatman filter paper, the extract was filtered and stored in the refrigerator. To synthesize ZnO using leaf extract, 2 g of Zn $(NO_3)_2{\cdot}6H_2O$ were added to 20 ml of leaf extract boiled at 60 °C. The mixture was then heated until it turned into a thick, yellow paste. After that, it was moved to a crucible and heated for 2 h in a furnace at 400 °C. The obtained ZnO samples were used for further characterization.

2.2 Characterization Studies

The XRD spectra were characterized by a Bruker D8 Advanced with CuKα (1.5406 Å). Functional group of the compound was examined by using Fourier Transform Infrared Spectroscopy (IR Tracer -100- Shimadzu). UV–Visible measurement was carried out using 3600 Plus Shimadzu. Kratos AXIS Ultra with a monochromatic Al X-ray source at 150 W was used to perform X-ray photoelectron spectroscopy (XPS) analyses. A Brukers Dimension FastScan Atomic Force Microscopy (AFM) system was used to perform additional analysis of the surface topography. The morphology was identified by field emission scanning electron microscopy (ZEISS SIGMA 300) and transmission electron microscopy (TALOS F200S G2). Cyclic voltammetry (CV), square wave voltammetry (SWV) and electrochemical impedance spectroscopy (EIS) electrochemical measurements were carried out using Squidstat plus (Admiral).

2.3 Electrode Preparation

The electrochemical analysis was carried out using a three-electrode setup: a platinum wire served as the counter electrode, a GCE acted as the working electrode, an Ag/AgCl electrode functioned as the reference electrode, and PBS served as the electrolyte. To disperse the ZnO NPs powder (5 mg), it was sonicated in ethanol for 1 h. After using alumina powder to polish it, the GCE was rinsed with DD water and ethanol. This led to the drop casting of 10 ml of ZnO suspension onto the GCE surface, followed by oven drying. This procedure was used for all subsequent electrochemical experiments. The 0.05 M Na_2HPO_4 and NaH_2PO_4 solutions were used to create the supporting electrolyte pH 7 solution (PBS).

3 Results and Discussion

3.1 Structural Studies

The XRD pattern for the synthetic ZnO NPs is shown in Fig. 1a. It is observed that all the peaks corresponding to the planes (100), (002), (101), (102), (110), (103), (200), (112), (201), (004) and (202) are confirming the formation of hexagonal wurtzite structure and matches with the JCPDS No: 89–7102 [47]. The high-intensity peak (101) is an indication of the anisotropic growth nature of the material. Also, the narrow peaks indicate that other impurities were not present in the prepared sample. The absorption spectrum of the green synthesized ZnO nanoparticles is shown in Fig. 1b. It is inferred that the ZnO NPs have a strong broadband absorption in the UV region from 200 to 400 nm and are highly transparent in the visible region. The band gap is calculated using (1). In this, the $(\alpha h\nu)^2$ is drawn against $(h\nu)$ for the captured absorption spectra and extra plotted to $\alpha = 0$ for getting the band gap value. The obtained band gap for the synthesized ZnO NPs is 3.33 eV [49].

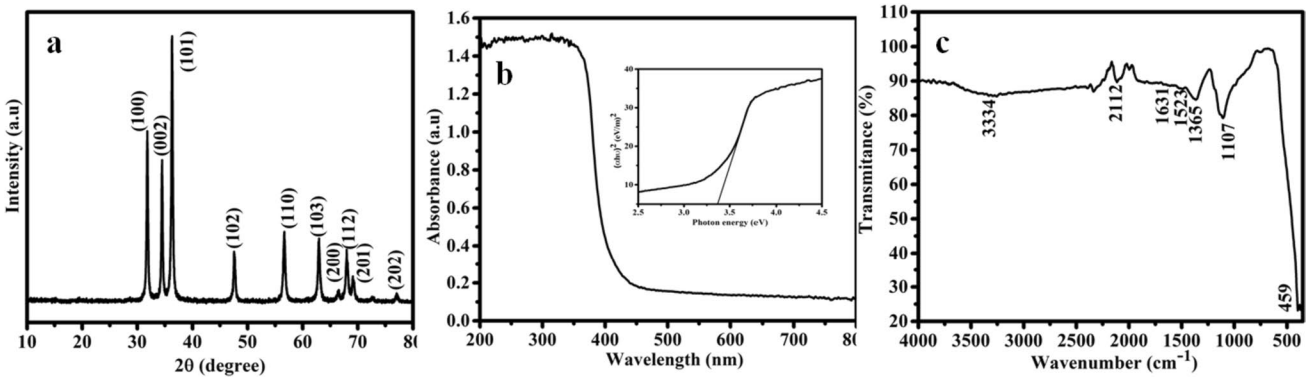

Fig. 1 ZnO NPs **a** XRD, **b** UV–Vis and **c** FTIR

$$\alpha h\nu = (h\nu - \lambda)^{1/2} \quad (1)$$

To study the functional groups and the formation of ZnO NPs FT-IR measurement is carried out from 400 to 4000 cm^{-1} and the corresponding spectra are shown in Fig. 1c. The absorption in the region from 400 to 600 cm^{-1} is due to metal–oxygen (Zn–O). It is observed that the M. *oleifera* structure is confirmed with the absorption band at 3334, 2112, 1523 1631, and 1107 cm^{-1} respectively [47, 50].

XPS analysis showed a better understanding of the chemical composition of the ZnO thin films derived from moringa leaves. The wide scan spectra showed the signatures of C 1 s, O 1 s, and Zn 2p as shown in Fig. 2a. Zn 2p describes the core level of the zinc atom which represents doublets peak in the highest binding energy. The deconvoluted fine scan spectra of C 1 s showed a presence of aliphatic carbon C–C at 285 eV, and other functional groups as C–O at 286.5 eV, and C=O at 287.6 eV in Fig. 2b [42–44].

The fine scan of O 1 s contains ZnO in the lowest binding energy of 530.2 eV, which clearly indicates that highly electronegative oxygen forms an ionic bond with an electropositive Zn^{2+} [45], due to Zn atom donates two valence electrons to the O atom which represents ZnO. Similar signature of sp^3 hybridized carbon with two functional groups as C–O and C=O/C–OH at 532.3 and 533.8 eV respectively in Fig. 2c. Interestingly, there is no presence of water, and it is due to the annealing of ZnO at 400 °C. XPS spectrum of Zn 2p reveals the two spin orbit components as Zn 2p3/2 and Zn 2p1/2 in the highest binding energy at 1021.9 eV and 1045.3 eV as shown in Fig. 2d [46].

3.2 Morphological Studies

AFM and FESEM nanoimaging is used to obtain the surface morphology of ZnO powder and their distribution. Flaky like uniform and dense morphology was observed from AFM as shown in Fig. 3a with a surface roughness of 2.3 nm. The scanning distance of ~ 420 nm showed a distribution of ZnO on the surface as shown in Fig. 3b. To investigate further, FESEM was employed to determine the porosity, grain size of ZnO as shown in Fig. 3c, d. FESEM confirms the rod and flake like morphology and the surface is inhomogeneous [47, 48]. The TEM image clearly describes the formation of spherical shaped nanoparticles for the prepared ZnO with an average size of 47 nm (Fig. 3e). The interplanar spacing of 0.284 nm, that compares to the (002) plane of hexagonal wurtzite and confirms the formation of the ZnO NPs, is shown in a lattice-resolved higher magnification TEM image in Fig. 3f.

3.3 Electrochemical Biosensor

GCE were initially cleaned using cyclic voltammetry analysis with potentials between − 0.45 and 0.45 V. SWV was used to calculate the electrode's selectivity for dopamine. Oxalic Acid (OA), glucose, and AA were added to a DA sensing system during an interference study using Chronoamperometric (CA) analysis at an applied potential of − 0.45 V. The Randles–Sevcik equation was used to calculate the effective surface area [51].

$$I_p = (2.69 \times 10^5)\, n^{3/2}\, A\, D^{1/2}\, C\, \upsilon^{1/2} \quad (2)$$

where Ip, n, A, D, and C, stood for the redox couple's peak current, the number of electrons involved in the reaction, the electrode's surface area, diffusion coefficient, the bulk solution's concentration in mol, and the scan rate, respectively. It was evident from the equation above that p was proportional to $\upsilon^{1/2}$, and the diffusion coefficient of dopamine was 5.5512×10^{-5} cm^2 s^{-1}.

Figure 4a reveals the cyclic voltammogram for different pH of PBS changes from 3 to 9. In that pH 7 proves high current compared with other pH. Figure 4b shows the cyclic voltammogram for bare GCE, ZnO modified GCE, and ZnO modified GCE in presence of 30 µM dopamine in PBS (pH 7) with the

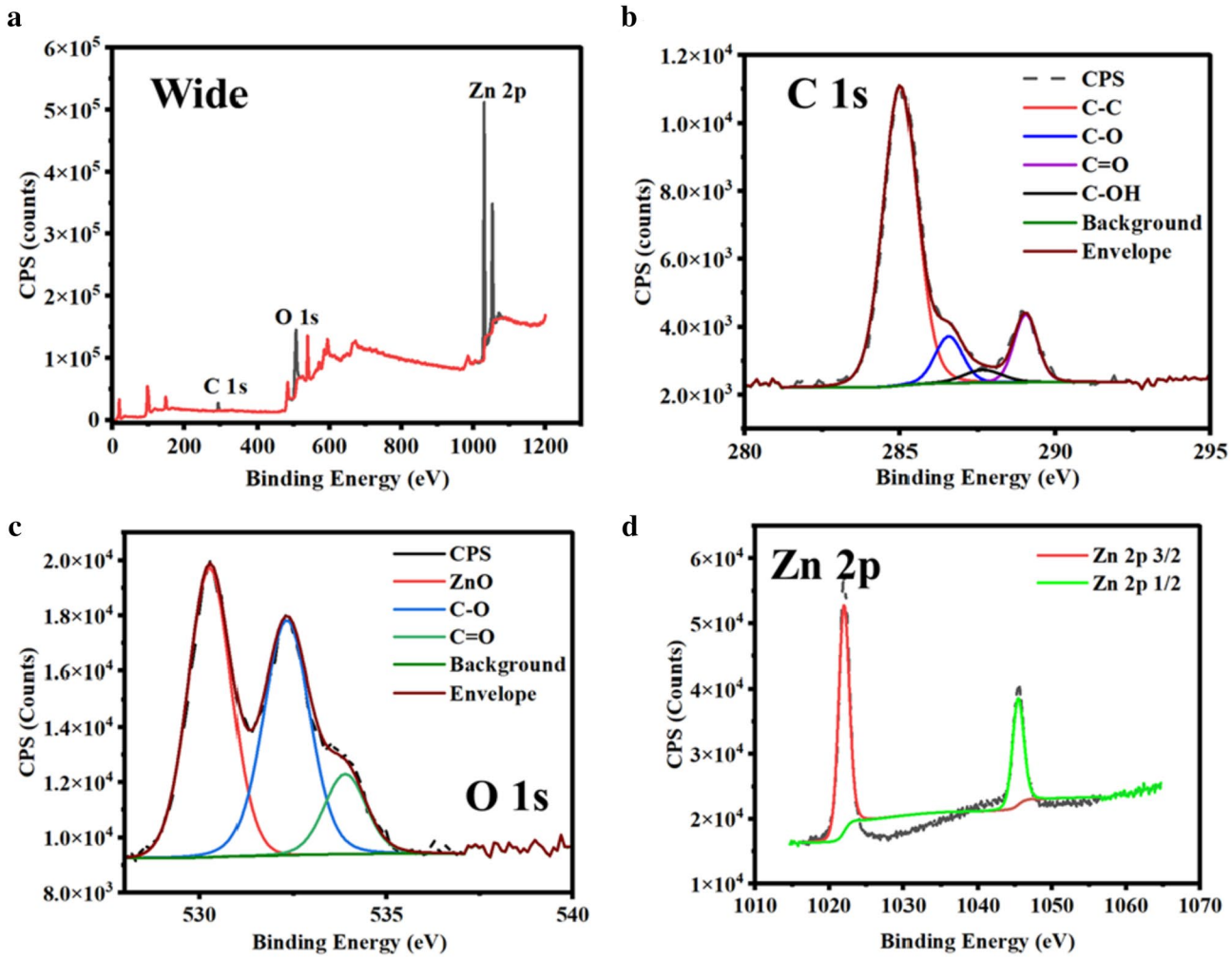

Fig. 2 Graphical representation of XPS analysis **a** Wide spectra; **b** C 1 s; **c** O 1 s; **d** Zn 2p

potential of − 0.45 to 0.45 V along the scan rate of 20 mV s^{-1}. We have not observed any oxidation or reduction peaks for GCE and ZnO modified GCE. Dopamine's oxidation and reduction produce a well-defined quasi-reversible redox couple with an oxidation peak potential of 0.35 V and a redox potential of 0.14 V, as shown in the figure [52]. Figure 4c shows the ZnO modified GCE towards dopamine in the concentration range between 15 and 30 µM. Peak currents for oxidation and reduction increase linearly as dopamine concentration rises. The rate transfer of the electrode (k_s) and number of electron involved in the electrochemical oxidation was calculated using Laviron's equation [51, 53, 54]

$$\log k_s = \alpha \log(1-\alpha) + (1-\alpha)\log\alpha - \log\left(\frac{RT}{nFv}\right) - \frac{nF\Delta E_p(1-\alpha)}{2.3RT} \quad (3)$$

$$I_p = n^2F^2vA\Gamma^*_o/4RT = nFQv/4RT \quad (4)$$

where α is the transfer coefficient (0.5), T is the ambient temperature, ΔE_{pa} is the redox potential's peak separation, and R is the ideal gas constant. In comparison to MWCNT/ZnO/Hb (1.22 s^{-1}) [55] and Hb immobilised at Nafion-coated, thermally synthesized ZnO on MWCNT (1.14 s^{-1}) [56] and GCE modified with ZnO, the k_s value for the modified GCE was calculated to be 1.32 s^{-1}. The number of electrons transferred during the electrode reaction, n, is given by the Eq. (3), where ν is the sweep rate, A is the modified electrode's effective surface area, I_p is the peak current, Q is the amount of charge, and F is the Faraday constant. Calculations show that only one electron-transfer reaction took place at the direct electron transfer reaction of dopamine, which transferred n = 1.1 electrons.

CV curve of 30 µM dopamine reported at diverse scan rate are presented in Fig. 3d. It is obvious that the oxidation of dopamine moderately rises as the scanning rates change from 10 to 50 mV s^{-1}. Dopamine's anodic peaks shift towards positive voltage direction as the potential scanning

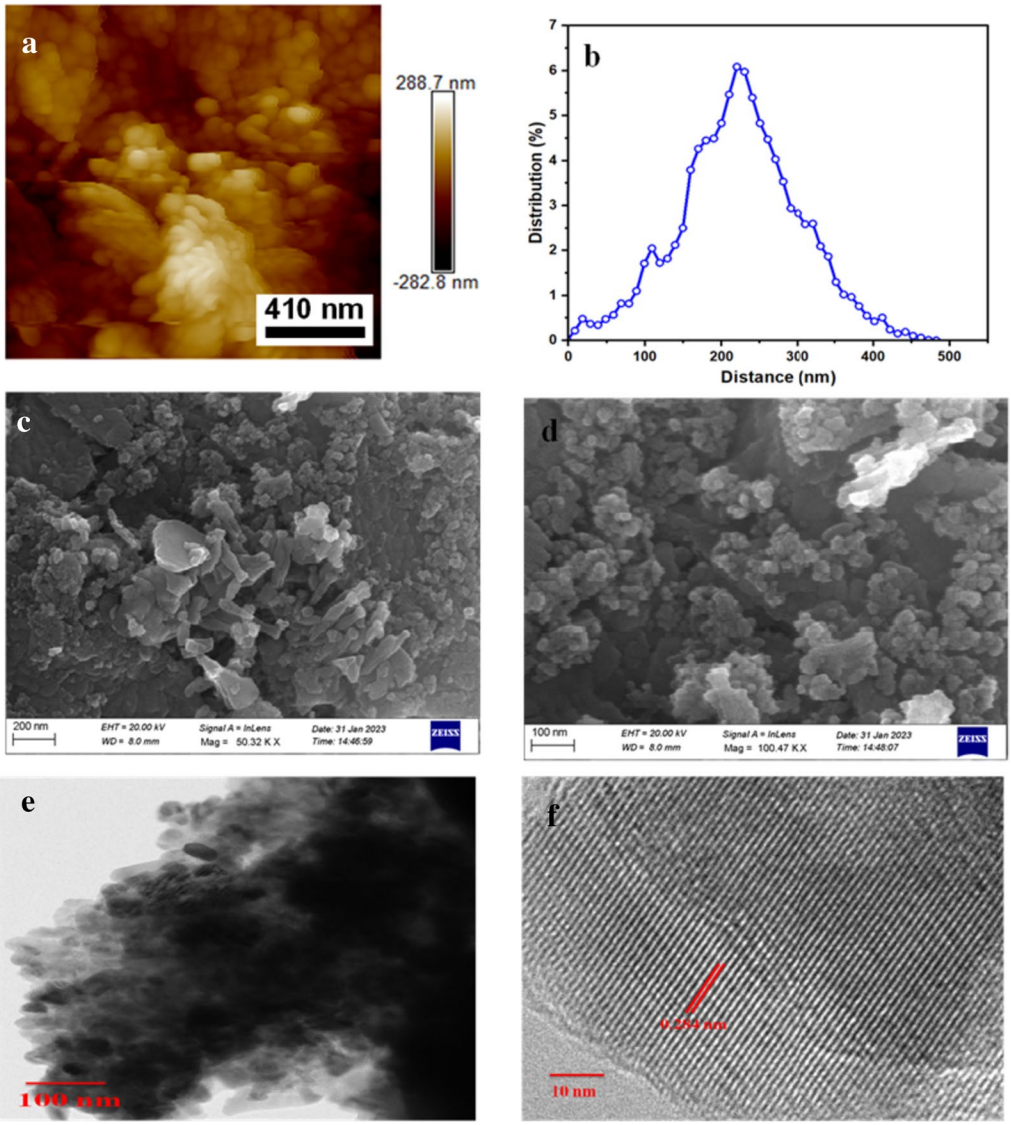

Fig. 3 ZnO NPs **a** AFM surface morphology **b** Graphical representation of distribution analysis of ZnO vs. distance, **c**, **d** FESEM image, **e** TEM image and **f** HRTEM image

increases, whereas its cathodic peaks shift in the opposite direction. The I_{pa}/I_{pc} is also very near 1, indicating a quasi-reversible process. According to Fig. 3e, both oxidation and reduction linearly increase as scanning rates, with good correlation coefficients (R2) of 0.9968 and 0.9934, demonstrating that the process is diffusion-controlled. According to a report, dopamine redox involves the transfer of two electrons [33, 57, 58].

3.4 Determination of DA

By using the oxidation peak currents of DA as analytical signals, CV was used to determine the DA at the ZnO modified GCE electrodes. The SWV curves for dopamine detection at the ZnO modified GCE are shown in Fig. 5a. When we examine the SWV curves, we can see that their currents grew as dopamine concentration increased while the oxidation potential remained constant. According to Fig. 5b, the linear range of the relationship between the current and dopamine concentration is 0.6–12 µM, and the linear regression equation is $I\ (A) = 2.0172x + 5.3392$, $R^2 = 0.9926$. We are able to determine from the linear regression equation that the sensitivity of the ZnO modified GCE electrode is 28.8172 $\mu A \mu M^{-1}\ cm^{-2}$ and the calculated limit of detection (LOD) is 0.3 µM. The performance of ZnO modified GCE electrode with other modified electrodes for the determination of dopamine is listed in Table 1.

For the biosensor's practical applications, selectivity is crucial because dopamine naturally coexists with a number of interfering species by using amperometric (i–t)

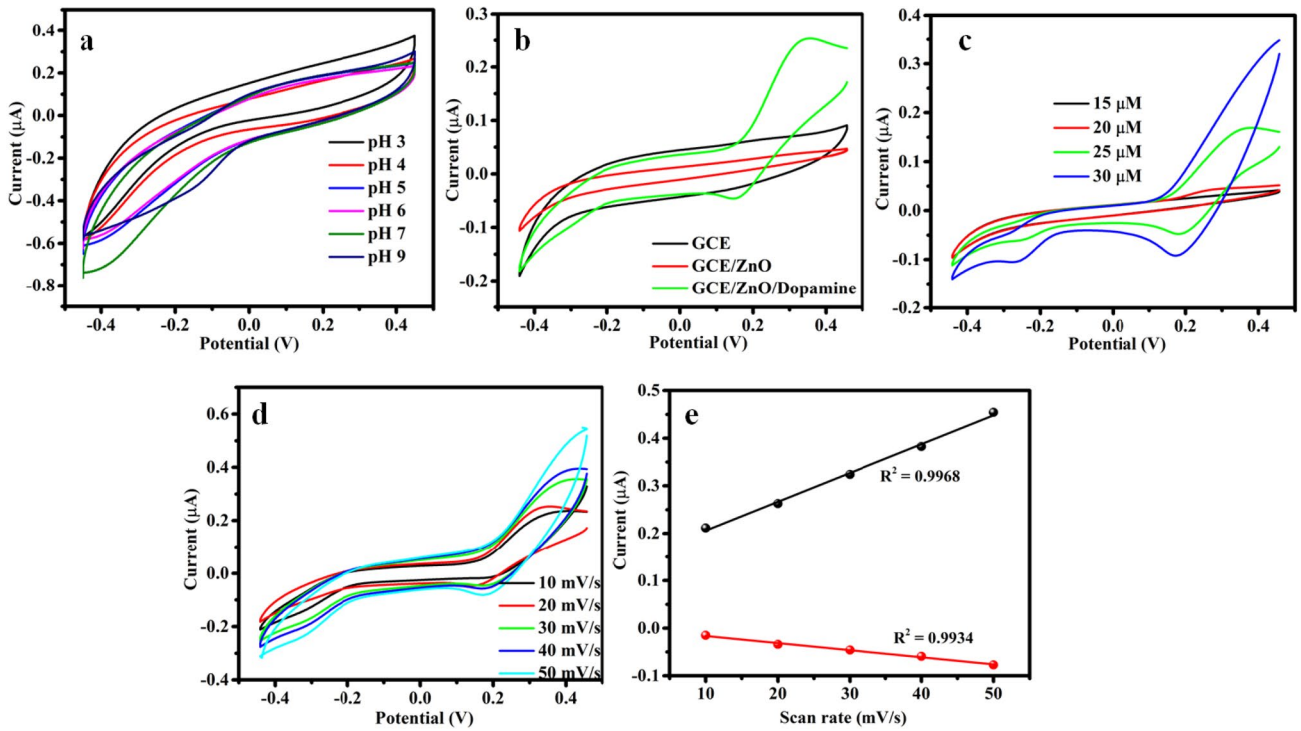

Fig. 4 **a** CV curves for different pH **b** cyclic voltammogram, **c** different concentration of dopamine, **d** 30 μM of dopamine at different scanning rate and **e** Linear plot of redox peaks current of dopamine *vs* scan rate

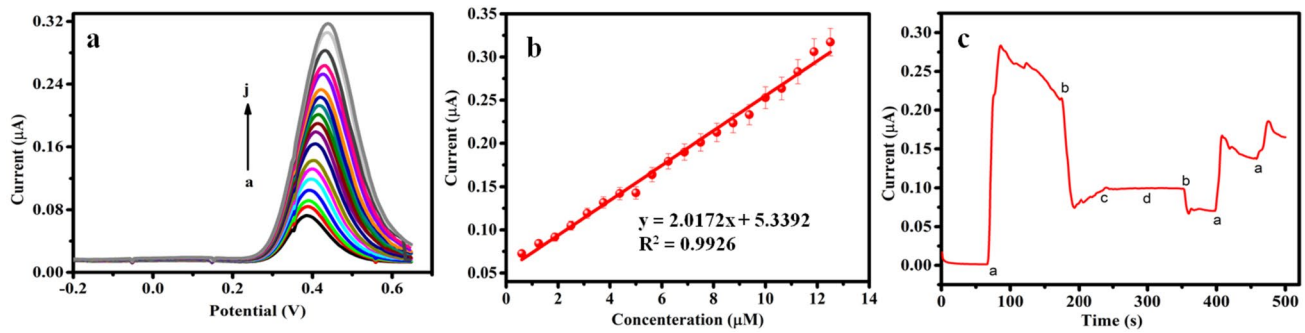

Fig. 5 **a** SWV curves for different dopamine concentrations, **b** a linear relationship between current and dopamine concentration, (the error bar denote standard deviation for n = 3) and **c** amperometric (i–t) responses in the presence of 25-fold excess solutions of oxalic acid, glucose, and ascorbic acid along with repeated additions of 10 M dopamine

Table 1 Functional groups presence in the synthesized ZnO NPs

Wavenumber (cm^{-1})	Functional group
459	Zn–O—bond bending vibration
3334, 1631	Hydroxyl group (O–H) in the water molecule
1365, 1107	Carboxylic C–O group
1523	Amide II region
2112–1631	Alkyne (C–C) and carbonyl (C=O)

techniques. We chose a 50-fold excess of typically interacting biological compounds for this evaluation such as oxalic acid, glucose, and ascorbic acid. As a result, we examined the selectivity of the ZnO modified GCE electrode in the presence of these typical electroactive species. The selectivity of the biosensor was assessed using the amperometric method. The electrode potential was maintained at 0.45 V while the supporting electrolyte solution (PBS) was

continuously stirred at 1200 rpm during the amperometric measurements.

The amount of dopamine taken into consideration for this study is 30 µM. The results of this study show that the presence of typical biological compounds that interface with cells has no effect on the oxidation signal of dopamine. The oxidation current signal of (a) dopamine in the presence of (b) oxalic acid (c) glucose, and (d) ascorbic acid, which are some of the common interfacing compounds are shown in Fig. 5c. The results of this study show that the presence of typical biological compounds that interface with cells has no effect on the oxidation signal of dopamine. Even in the presence of common interfacing compounds, we saw exactly the same oxidation current signal for dopamine, and this analysis is evidence of the high selectivity of the ZnO modified GCE. Scheme 1 represents the decomposition of DA into DOQ. Dopamine undergoes two electron processes during redox. Protons (H^+) and electrons (e^-) are involved in the dopamine redox process in equal amounts. Consequently, it can be deduced that the oxidation of dopamine involves the transfer of two electrons (2 e^-) coupling with two protons (2 H^+), in agreement with earlier research [54]. ZnO NPs enhanced the electron transfer between the electrolyte and the electrode.

Figure 6 displays EIS curve for GCE, ZnO modified GCE, GCE/dopamine and ZnO modified GCE/dopamine in 0.1 M KCl containing 0.5 mM $Fe(CN6)^{3-/4-}$. The experimental data was fitted using Randles equivalent circuit as been shown in inset Fig. 6, where R_s, R_{ct}, C_{dl}, and W stood for Warburg impedance, double layer capacitance, charge transfer resistance, and electrolyte resistance, respectively. We can see that the ion diffusion resistance corresponds to the three distinct regions of high-frequency, mid-frequency, and low-frequency. A single semicircle was visible in the centre, revealing the solution resistance at the intersection of the semicircle in the high-frequency region and the charge

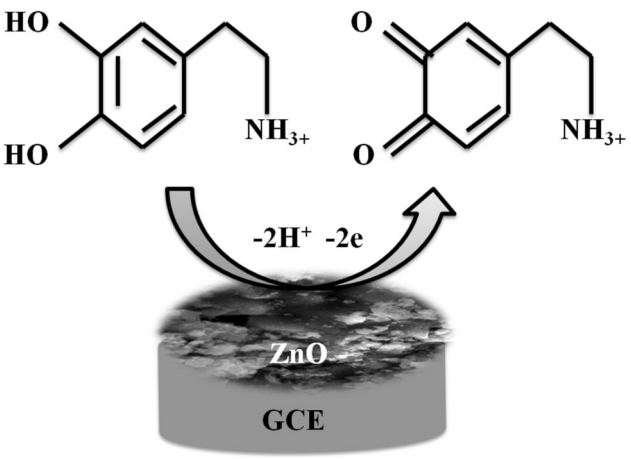

Scheme 1 Proposed mechanism for dopamine at ZnO modified GCE

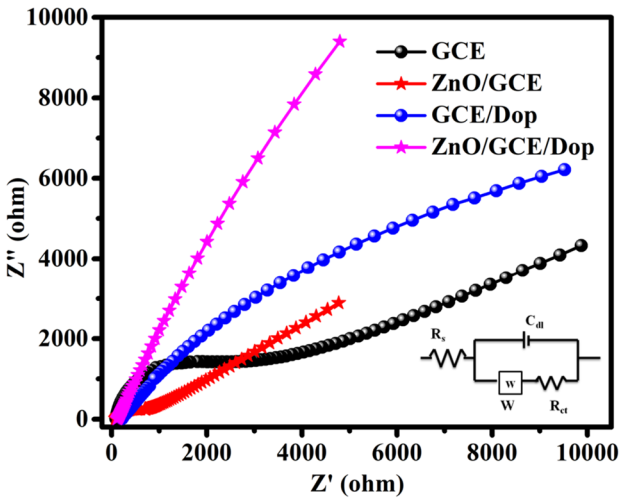

Fig. 6 EIS curve of ZnO modified GCE and ZnO/GCE/dopamine

transfer resistance (R_{ct}) at the interface, respectively. The R_{ct} values was observed at the ZnO modified GCE (708 Ω) was much smaller than those of GCE (2821 Ω), which indicates a lower diffusion resistance and charge transfer resistance. Because of this, the ZnO modified GCE has a smaller semicircle than the bare electrode, proving that it is a good electrical conductive material and it also appropriate for electrochemical applications.

3.5 Stability, Repeatability and Reproducibility of Electrochemical Sensor

First we conducted the stability of dopamine biosensor has been verified by carrying out testing at the regular interval of a week and it has been found that ZnO modified GCE electrode based electrochemical biosensor retains its 96% activity after 21 days. The excellent reproducibility of the ZnO modified GCE electrodes were later confirmed by this study. Five independent ZnO modified GCE with an RSD of 3.42% for the detection of dopamine was used to evaluate the electrochemical sensor's reproducibility. We performed repeatability studies using a single ZnO modified GCE electrode. For this, five consecutive measurements were taken with a relative standard deviation (RSD) of 3.36%. The excellent repeatability of the electrochemical sensor was confirmed by this study.

3.6 Real Time Applicability

With their consent, urine samples were taken from volunteers in good health at Vellore Institute of Technology Chennai. The urine sample was filtered using cellulose nitrate filter paper. 19.5 mL of 0.1 M PBS is thoroughly mixed with 0.5 mL of urine samples. ZnO NPs were employed in

Table 2 Comparative analysis of performance of green synthesized ZnO modified GCE with other electrodes/techniques for the detection of dopamine

Electrodes	Techniques	LOD (μM)	Sensitivity ($\mu A \mu M^{-1} cm^{-2}$)	Linear range (μM)	References
O/GCE	DPV	0.04	4.38	0.1–16	[52]
ZnO/ERGO/GCE	SDLSV	0.0036	28.452	0.01–80	[33]
Au-ZnO/GF	DPV	0.04	4.36	0–80	[57]
ZnO/MWCNTs/GCE	CV	1	0.785	0–300	[58]
ZnO/GCE	SWV	0.03	28.8172	0.6–12	This work

the amperometric tests for the best possible experimental conditions. The recovery test results are listed in Table 2. An average recovery value of 97.6–98.2% and the current relative standard deviation among recovery is 0.4–0.9 is found for the sensor. The findings demonstrate the great potential of the proposed ZnO/GCE for real-time dopamine sensing.

Sample	Added (μM)	Found (μM)	Recovery (%)	RSD (%)
Urine sample	10	9.7	97	0.8
	12.5	12.25	98	0.4
	15	15.15	101	0.9

4 Conclusions

The investigation into the detection of dopamine through the utilization of ZnO nanoparticles synthesized using green methods offers a potentially promising path for the advancement of sensor technology with a focus on environmental sustainability. The prepared ZnO NPs electrode shows an excellent electrochemical performance for the detection of dopamine such as wide linear range of 0.6–12 μM, high sensitivity of 28.81 $\mu A \mu M^{-1} cm^{-2}$ at the low detection limit of 0.03 μM. In comparison to the works reported in the literature, the green-synthesized ZnO based electrochemical sensor proposed shows superior performance for the detection of dopamine. Furthermore, the outcomes suggest that the biosensor, in its current state of preparation, offers up new possibilities for determining various types of biomolecules. The suggested effort emphasizes responsible and sustainable scientific advancement in sensor technology to advance neuroscience, clinical diagnostics, and other fields.

Acknowledgements Authors are much thankful to Vellore Institute of Technology, Chennai for providing "VIT RGEMS SEED GRANT" for carrying out this research work.

Author Contributions Author 1 (MM): Material synthesis, data collection, TEM, FESEM and electrochemical analysis. Author 2 (GLP): Conceived the proposed idea, contributed to the study conception, methods, and material selection. Author 3 (EM): XRD, FT-IR, UV–Vis characterization studies. Author 4 (VS): XPS, AFM analysis. All the authors have contributed to the overall paper drafting, extraction of results and editing work for their respective sections. All authors reviewed the manuscript.

Funding Authors are much thankful to Vellore Institute of Technology, Chennai for providing "VIT RGEMS SEED GRANT" for carrying out this research work.

Data Availability Not Applicable.

Code Availability Not applicable.

Declarations

Competing Interests The authors declare that they have no known competing financial interests or personal relationships that could have appeared to influence the work reported in this paper.

Ethical Approval The manuscript is prepared as per the ethical standard of the journal.

Consent to Participate Not Applicable.

Consent for Publication The authors has given Consent for Publication as per the journal policy.

References

1. M.M. Ahmed, R. Zhao, J. Du, J. Li, J. Electrochem. Soc. **169**, 20573 (2022)
2. S. Tajik, H. Beitollahi, S.Z. Mohammadi, M. Azimzadeh, K. Zhang, Q. Van Le, Y. Yamauchi, H.W. Jang, M. Shokouhimehr, RSC Adv. **10**, 30481 (2020)
3. H. Beitollahi, M. Safaei, S. Tajik, Anal. Bioanal. Chem. Res. **6**, 81 (2019)
4. N. Atta, A. Galal, F. Abu-Attia, S. Azab, J. Electrochem. Soc. **157**, F116 (2010)
5. R. Tandel, S. Pawar, S. Jaldappagari, J. Electrochem. Soc. **163**, H705 (2016)
6. S. Yasmin, M.S. Ahmed, D. Park, S. Jeon, J. Electrochem. Soc. **163**, B491 (2016)
7. G. Li, P. Zhong, Y. Ye, X. Wan, Z. Cai, S. Yang, Y. Xia, Q. Li, J. Liu, Q. He, J. Electrochem. Soc. **166**, B1552 (2019)
8. S. Singh, M.R. Hasan, P. Sharma, J. Narang, Sens. Int. **3**, 100190 (2022)
9. S. Tajik, H. Beitollahi, F.G. Nejad, M. Safaei, K. Zhang, Q. Van Le, R.S. Varma, H.W. Jang, M. Shokouhimehr, RSC Adv. **10**, 21561 (2020)
10. N. Anzar, R. Hasan, M. Tyagi, N. Yadav, J. Narang, Sens. Int. **1**, 100003 (2020)

11. F. Garkani Nejad, S. Tajik, H. Beitollahi, I. Sheikhshoaie, Talanta **228**, 122075 (2021)
12. M. Gerard, A. Chaubey, B.D. Malhotra, Biosens. Bioelectron. **17**, 345 (2002)
13. C.B.A. Hassine, H. Kahri, H. Barhoumi, J. Electrochem. Soc. **167**, 27516 (2020)
14. L. Gao, J. Ma, J. Zheng, J. Electrochem. Soc. **167**, 107503 (2020)
15. H.R. Ghorbani, F.P. Mehr, H. Pazoki, B.M. Rahmani, Orient. J. Chem. **31**, 1219–1221 (2015)
16. P. Sharma, M.R. Hasan, N.K. Mehto, A.B. Deepak, J. Narang, Sens. Int. **3**, 100182 (2022)
17. P. Sharma, H. Hassan, M.R. Hasan, T. Fatima, H. Mohan, M. Khanuja, S. Kaushik, J. Narang, Biosens. Bioelectron. X **13**, 100303 (2023)
18. N.K. Mehto, P. Sharma, S. Kumar, M. Khanuja, R. Rawal, J. Narang, Process Biochem. **123**, 36 (2022)
19. B.D. Malhotra, A. Chaubey, Sens. Actuators B Chem. **91**, 117 (2003)
20. N. Anzar, M. Rahil Hasan, M. Akram, N. Yadav, J. Narang, Process Biochem. **94**, 126 (2020)
21. N. Anzar, S. Suleman, H. Bano, S. Parvez, M. Khanuja, R. Pilloton, J. Narang, Sensors **23**, 5519 (2023)
22. J.N. Hasnidawani, H.N. Azlina, H. Norita, N.N. Bonnia, S. Ratim, E.S. Ali, Procedia Chem. **19**, 211 (2016)
23. P.P. Mahamuni, P.M. Patil, M.J. Dhanavade, M.V. Badiger, P.G. Shadija, A.C. Lokhande, R.A. Bohara, Biochem. Biophys. Rep. **17**, 71 (2019)
24. S. Sharma, S.S. Pande, P. Swaminathan, RSC Adv. **7**, 39411 (2017)
25. S. Srujana, D. Bhagat, Nanotechnol. Environ. Eng. **7**, 269 (2022)
26. G. Ghoshal, M. Singh, Mater. Sci. Energy Technol. **5**, 22 (2022)
27. J.O. Primo, C. Bittencourt, S. Acosta, A. Sierra-Castillo, J.F. Colomer, S. Jaerger, V.C. Teixeira, F.J. Anaissi, Front. Chem. **8**, 1 (2020)
28. N. Matinise, X.G. Fuku, K. Kaviyarasu, N. Mayedwa, M. Maaza, Appl. Surf. Sci. **406**, 339 (2017)
29. S. Faisal, H. Jan, S.A. Shah, S. Shah, A. Khan, M.T. Akbar, M. Rizwan, F. Jan, N. Wajidullah, A.K. Akhtar, S. Syed, ACS Omega **6**, 9709 (2021)
30. S. Saeed, S. Nawaz, A. Nisar, T. Mehmood, M. Tayyab, M. Nawaz, S. Firyal, M. Bilal, A. Mohyuddin, A. Ullah, Mater. Res. Express **8**, 35004 (2021)
31. M.S. Lakshmi Prabha Chandrasekar, B.D. Sethuraman, S. Mohandos, Int. J. Environ. Anal. Chem. **8**, 1 (2023)
32. W.H. Zhou, H.H. Wang, W.T. Li, X.C. Guo, D.X. Kou, Z.J. Zhou, Y.N. Meng, Q.W. Tian, S.X. Wu, J. Electrochem. Soc. **165**, G3001 (2018)
33. F. Li, B. Ni, Y. Zheng, Y. Huang, G. Li, Surf. Interfaces **26**, 101375 (2021)
34. J. Lin, B. Huang, Y. Dai, J. Wei, Y. Chen, Mater. Sci. Eng. C **93**, 739 (2018)
35. S. Verma, P. Arya, A. Singh, J. Kaswan, A. Shukla, H.R. Kushwaha, S. Gupta, S.P. Singh, Biosens. Bioelectron. **165**, 112347 (2020)
36. C. Nong, B. Yang, X. Li, S. Feng, H. Cui, Int. J. Electrochem. Sci. **17**, 220331 (2022)
37. J.K. Shashikumara, B.E.K. Swamy, S.C. Sharma, S.A. Hariprasad, K. Mohanty, Sci. Rep. **11**, 14310 (2021)
38. C. Yang, C. Zhang, T. Huang, X. Dong, L. Hua, J. Mater. Sci. **54**, 14897 (2019)
39. S. Tajik, H. Beitollahi, H.W. Jang, M. Shokouhimehr, Talanta **232**, 122379 (2021)
40. S. Tajik, Y. Orooji, F. Karimi, Z. Ghazanfari, H. Beitollahi, M. Shokouhimehr, R.S. Varma, H.W. Jang, J. Food Meas. Charact. **15**, 4617 (2021)
41. S. Tajik, M.A. Taher, H. Beitollahi, Ionics **20**, 1155 (2014)
42. M.M. Foroughi, H. Beitollahi, S. Tajik, A. Akbari, R. Hosseinzadeh, Int. J. Electrochem. Sci. **9**, 8407 (2014)
43. A. Munawar, F. Zafar, S. Majeed, M. Irfan, H. Ullah Khan, G. Yasmin, N. Akhtar, J. Electroanal. Chem. **895**, 115469 (2021)
44. G. Qu, G. Fan, M. Zhou, X. Rong, T. Li, R. Zhang, J. Sun, D. Chen, ACS Omega **4**, 4221 (2019)
45. A. Sahai, N. Goswami, AIP Conf. Proc. **1665**, 0500 (2015)
46. Z. Li, H. Chen, W. Liu, Catalysts **8**, 557 (2018)
47. K. Elumalai, S. Velmurugan, Appl. Surf. Sci. **345**, 329 (2015)
48. S.A. Al-Zahrani, M.B. Patil, S.N. Mathad, A.Y. Patil, A.A. Otaibi, N. Masood, D. Mansour, A. Khan, A. Manikandan, E. Syafri, Crystals **13**, 577 (2023)
49. S.S. Kanmani, K. Ramachandran, S. Umapathy, Int. J. Photoenergy **2012**, 1 (2012)
50. D. Letsholathebe, F.T. Thema, K. Mphale, K. Maabong, C.M. Magdalane, Mater. Today Proc. **38**, 2445 (2020)
51. M. Manikandan, C. Revathi, P. Senthilkumar, S. Amreetha, S. Dhanuskodi, R.T. Rajendra Kumar, Ionics **26**, 2003 (2020)
52. D. Balram, K.Y. Lian, N. Sebastian, Int. J. Electrochem. Sci. **13**, 1542 (2018)
53. M. Manikandan, S. Dhanuskodi, N. Maheswari, G. Muralidharan, C. Revathi, R.T. Rajendra Kumar, G. Mohan Rao, Sens. Bio-Sens. Res. **13**, 40 (2017)
54. M. Ognjanović, D.M. Stanković, M. Jović, M.P. Krstić, A. Lesch, H.H. Girault, B. Antić, A.C.S. Appl, Nano Mater. **3**, 4654 (2020)
55. S. Palanisamy, S. Cheemalapati, S.M. Chen, Anal. Biochem. **429**, 108 (2012)
56. W. Ma, D. Tian, Bioelectrochemistry **78**, 106 (2010)
57. H.Y. Yue, H.J. Zhang, S. Huang, X.X. Lu, X. Gao, S.S. Song, Z. Wang, W.Q. Wang, E.H. Guan, Mater. Sci. Eng. C **108**, 110490 (2020)
58. S.S.J. Aravind, S. Ramaprabhu, Nanosci. Methods **1**, 102 (2012)